Regular Article

PHYSICAL CHEMISTRY RESEARCH
Published by the
Iranian Chemical Society
www.physchemres.org
info@physchemres.org

Phys. Chem. Res., *Vol. 2, No. 1, 21-29, June 2014.*
DOI: 10.22036/pcr.2014.3816

Crystal Chemistry of Immobilization of Tetravalent Ce and Se in Ceramic Matrix of Sodium Zirconium Phosphates

A. Bohre*, O.P. Shrivastava and K. Awasthi
Department of Chemistry, Dr H.S. Gour University, Sagar 470003 India
(Received 2 August 2013, Accepted 7 November 2013)

Sodium zirconium phosphate (here after NZP) is a typical host material capable of converting the intermediate level waste resulting from light water reactor (LWR) fuel reprocessing into a single-phase material with good stability, high integrity and long durability. The crystal chemistry of $NaZr_{1.9}Ce_{0.1}P_3O_{12}$ and $NaZr_{1.9}Se_{0.1}P_3O_{12}$ phases has been investigated using general structure analysis system programming. The Se/CeNZP phases crystallize in the space group *R*-3c and Z = 6. Powder diffraction data have been subjected to Rietveld refinement to arrive at a satisfactory structural convergence of R-factors. The Phosphate counter ions stretching and bending vibrations in the infrared (IR) region have been assigned. SEM and EDAX analyses provide evidence of Ce and Se in the matrix.

Keywords: Ceramic, Se/CeNZP, Powder XRD, GSAS, Rietveld refinement

INTRODUCTION

The safe and effective management of radioactive waste has been given utmost importance from the very inception of nuclear industry in India and it covers the entire range of activities from handling, treatment, conditioning, transport, storage and finally disposal. Radioactive waste is generated at various stages of the nuclear fuel cycle, which includes the mining and milling of uranium ore, fuel fabrication, reactor operation and spent fuel reprocessing [1-3]. Beside these sources, radioactive waste is produced as a result of the ever-increasing use of radioisotopes in medicine, industry and agriculture [4-5].

Intermediate-level radioactive waste (ILW) generated from light water reactor (LWR) spent fuel reprocessing (commercial waste) or from weapons technology (government waste) may require solidification and incorporation into an inert and durable host matrix suitable for deep geologic disposal [6-7]. The selected host matrix must have high chemical stability, radiation resistance and thermo-mechanical integrity during long-term (10^5-10^6 years) disposal. The major nuclear waste forms can be considered as belonging to three groups, *viz.* glasses, titanates and phosphates of various compositions. Glass and its derivatives have long been considered as host matrices for ILW because of their adequate durability. The main disadvantage of glass is its thermodynamic instability, which appears during high-temperature crystallization caused by radioactive decay. In this case, mechanical and chemical properties of glasses are deteriorated [8-9].

Among the phosphate materials, sodium zirconium phosphate, $NaZr_2P_3O_{12}$ (NZP), structural family is being studied as a waste form. The capacity for an enormous range of crystal-chemical substitutions in the NZP structure makes it a significant host for accommodating a wide range of radionuclides [10-11]. The compounds of this family exhibit characteristic properties such as radiation damage resistance, low thermal expansion [12], low leaching of ions, and *etc.* Compounds of NZP family are represented by the general crystal-chemical formula $(M1)(M2)_3\{[L_2(TO_4)_3]^{p-}\}_{3\infty}$, where M1 and M2 represent the two distinct empty sites in the framework. The structure consists of network of corner sharing LO_6 octahedrons and TO_4 tetrahedrons. The structural unit consisting of two octahedrons and three tetrahedrons $\{[L_2(TO_4)_3]^{p-}\}$ are connected in the form of ribbons parallel to the *c-axis* of the

*Corresponding author. E-mail: ashish.bohre@gmail.com

unit cell. These ribbons are linked together perpendicular to the *c-axis* by TO_4 tetrahedrons to build the three-dimensional framework [13-14]. Because of the availability of different crystallographic sites for substitution in the NZP structure, the structure is highly flexible with respect to isomorphic substitutions. Hence, it is possible to obtain a single phase NZP waste form comprising most of the radioactive elements. This may probably eliminate the difficulties such as thermodynamic incompatibilities, differential expansion, differential leaching of ions, and *etc*. [15-16].

The present communication demonstrates the scientific feasibility of selenium and cerium immobilization in the NZP matrix through an acceptable structure model based on the refinement of crystallographic data. It also investigates the crystallochemical changes due to matrix modification when tetravalent cations like Ce^{4+} and Se^{4+} are substituted for zirconium site of the NZP framework.

EXPERIMENTAL

Ceramic Route Synthesis of $NaZr_{1.9}Ce_{0.1}P_3O_{12}$ and $NaZr_{1.9}Se_{0.1}P_3O_{12}$ Phases

In the present work, the solid solutions of $NaZr_{1.9}Ce_{0.1}P_3O_{12}$ and $NaZr_{1.9}Se_{0.1}P_3O_{12}$ were synthesized by conventional solid state reaction method. Stoichiometric quantity of dry fine powders of precursor nitrates, carbonates and ammonium dihydrogen phosphate were mixed in a mortar-pestle in glycerol medium. The selected chemical compounds were AR grade Na_2CO_3, SeO_2, CeO_2, $ZrO(NO_3)_2$ and $(NH_4)H_2PO_4$. The glycerol paste was gradually heated initially at 600 ºC for 8 h in a platinum crucible. The initial heating is done to decompose Na_2CO_3 and $(NH_4)H_2PO_4$ with the evolution of NO_x, carbon dioxide gases, ammonia and water vapors. The powders were then compacted into small discs of 12.5 mm diameter and 2-3 mm of thickness under a load of 4 tons. Then pellets were sintered in a platinum crucible at 1250 ºC for 72 h.

Characterization

The phase purity of the synthesized samples was checked by X-ray diffraction on PANalytical diffractometer (XPERT-PRO) with VANTEC detector using CuKα radiation ($\lambda = 1.54060$ Å) at a step size of $2\theta = 0.02^\circ$ and a fixed counting time of 5 s/step and were refined by the Rietveld method using the GSAS program. The homogeneity and chemical compositions of the samples were checked by scanning electron microscopy (SEM). SEM has been carried out on an electron microscope system (ZEISS) equipped with thermonoran ultra dry detector facility for energy dispersive X-ray (EDAX) analysis. The images presented are recorded in backscattered electron (BSE) mode and electrons with energy 20 keV were used in all experiments. To confirm functional compositions of the phosphates, their IR spectra were recorded using a SHIMADZU FTIR-8400S instrument. Samples were prepared by finely dispersing powder material on a KBr carrier.

RESULTS AND DISCUSSION

Rietveld Refinement and Crystallographic Model of the Phases

The powder XRD data showed that mono-phases of composition $NaSe_{0.1}Zr_{1.9}P_3O_{12}$ and $NaCe_{0.1}Zr_{1.9}P_3O_{12}$ are isostructural with $NaZr_2(PO_4)_3$ (Fig. 1) [17]. NZP crystallizes in the rhombohedral system (Space group R-3c). The conditions for the rhombohedral lattice: (i) $-h + k + l = 3n$ (ii) when $h = 0$, $l = 2n$ and (iii) when $k = 0$, $l = 2n$ have been verified for all reflections between $2\theta = 10^o$-120^o. The intensity and positions of the diffraction pattern match with the characteristic pattern of parent compound sodium zirconium phosphate, which gives several prominent reflections between $2\theta = 13.98^o$-46.47^o [18]. The general structure analysis system (GSAS) [19] program with the EXPGUI [20] graphical user interface was used for Rietveld [21] analysis of the X-ray powder diffraction data. High quality powder diffraction data in combination with the Rietveld method allows refinement of a structural model (atomic coordinates, site occupancies and atomic displacement parameters) as well as the profile parameters (lattice constants, peak shape, sample height, instrument parameters and background).

The structure refinement leads to rather good agreement between the experimental and calculated XRD pattern (Fig. 2) and yields acceptable reliability factors: RF^2, R_p and R_{wp} [22]. The normal probability plot for the histogram gives nearly a linear relationship indicating that the I_o and I_c

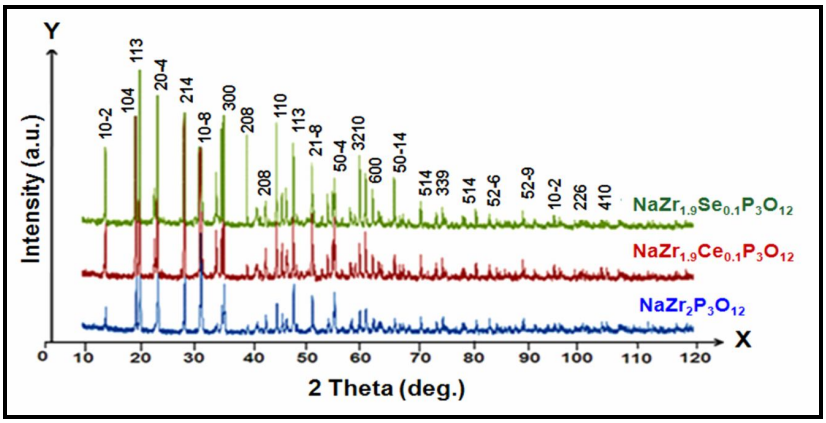

Fig. 1. Powder XRD pattern of $NaCe_{0.1}Zr_{1.9}P_3O_{12}$ and $NaSe_{0.1}Zr_{1.9}P_3O_{12}$ ceramic samples.

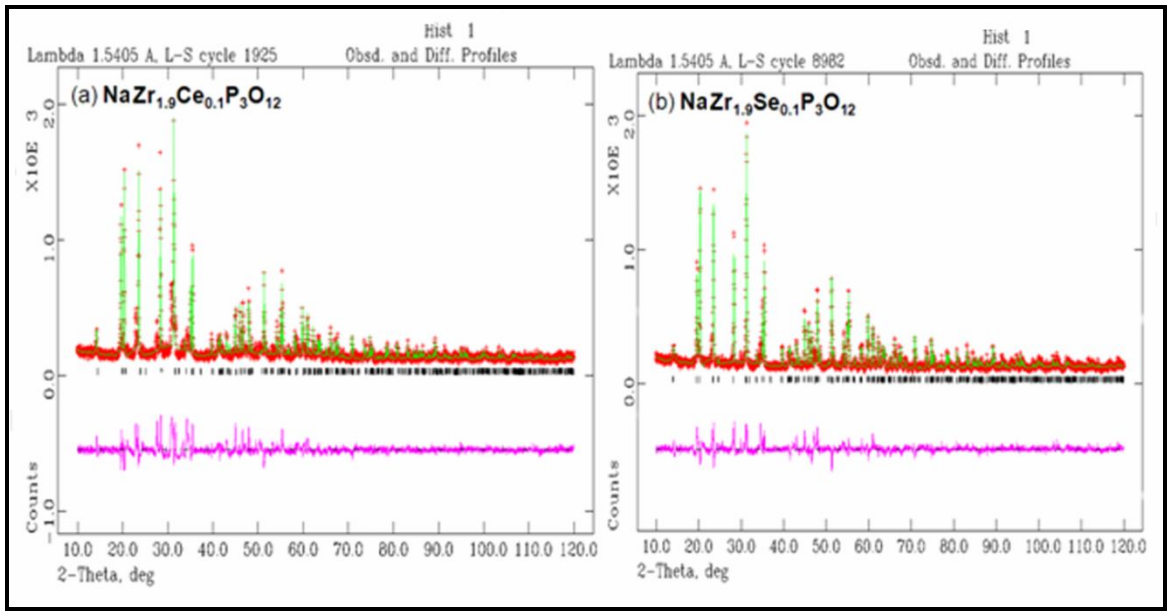

Fig. 2. (a and b) Rietveld refinement plot for $NaCe_{0.1}Zr_{1.9}P_3O_{12}$ and $NaSe_{0.1}Zr_{1.9}P_3O_{12}$ ceramic samples showing observed (+), calculated (continuous line) and difference (lower) curves. The vertical bars denote Bragg reflections of the crystalline phases.

values for the most part are normally distributed (Fig. 3). The lattice parameters are close to the corresponding values for un-substituted NZP unit cell [23]. The substitution of Zr^{4+} cation by tetravalent Se^{4+} and Ce^{4+} cations causes elongation of the unit cell along *c-axis*. Along the *a-axis* the unit cell shrinks (Table 1) [24]. Alteration in lattice parameters shows that the network modifies its dimensions to accommodate the cations without breaking the bonds [25]. The basic framework of NZP accepts cations of different sizes and oxidation states to form solid solutions but at the same time retaining the same overall geometry. The final atomic coordinates and isotropic thermal

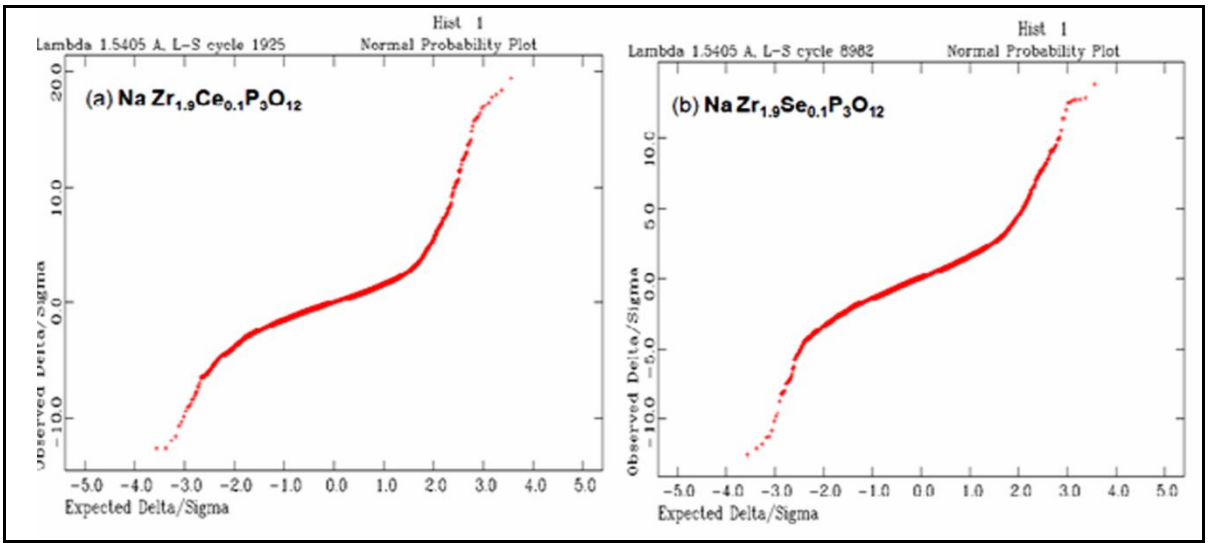

Fig. 3. (a and b) Probability plot between observed intensity (I_0) and calculated intensity (I_C) for $NaCe_{0.1}Zr_{1.9}P_3O_{12}$ and $NaSe_{0.1}Zr_{1.9}P_3O_{12}$ceramic samples.

Table 1. Crystallographic Data for Ceramic Phases $NaZr_{1.9}Ce_{0.1}P_3O_{12}$ and $NaZr_{1.9}Se_{0.1}P_3O_{12}$

Parameters	$NaZr_{1.9}Ce_{0.1}P_3O_{12}$	$NaZr_{1.9}Se_{0.1}P_3O_{12}$
Lattice constants		
a = b		
c	8.8212(12)	8.8019(17)
Rp	22.7772(5)	22.7878(6)
Rwp	0.0781	0.0727
$R_{expected}$	0.1075	0.1105
RF^2	0.0564	0.0597
Volume of unit cell	0.10215	0.13310
S (GoF)		
DWd	1531.31(4)	1537.82(7)
Unit cell formula weight	1.05	1.08
$Density_{X\text{-}ray}$ (g cm^{-3})	0.971	0.920
Slope	2751.53	2889.51
	3.17	3.21
	1.31	1.33

Structure: Rhombohedral, Space group: R-3c, Z: 6, α = β = 90º, γ = 120º

$$R_p = \frac{\sum y_i(obs) - y_i(cal)}{\sum y_i(obs)} \quad R_{wp} = \left\{ \frac{\sum w_i(y_i(obs) - y_i(cal))^2}{\sum w_i(y_i(obs))^2} \right\}^2 \quad R_e = \left[(N-P) / \sum w_i y_{oi}^2 \right]^{1/2}$$

$S = R_{wp}/R_{exp}$

$y_{i\,(o)}$ and $y_{i(c)}$ are observed and calculated intensities at profile point *i*, respectively. w*i* is a weight for each step *i*. N is the no of parameters refined.

parameters (Table 2), inter-atomic distances, (Table 3) and bond angles (Table 4) are extracted from the crystal information file (CIF) prepared after final cycle of refinement. The refinement leads to acceptable Zr-O and P-O bond distances. Zr atoms are displaced from the center of the octahedron due to the Na^{+}-Zr^{4+} repulsions. Consequently, the Zr-O(2) distance, neighboring the sodium Na, is slightly greater than the Zr-O(1) distance, however, average Zr-O distances are smaller than the values calculated from the ionic radii data (2.12 Å) [26].

Table 2. Refined Atomic Coordinates of $NaZr_{1.9}Ce_{0.1}P_3O_{12}$ and $NaZr_{1.9}Se_{0.1}P_3O_{12}$ Polycrystalline Solid Solutions at Room Temperature

Atom	x	y	z	Occupancy	U_{iso} ($Å^2$)
$NaZr_{1.9}Ce_{0.1}P_3O_{12}$					
Na1	0.0	0.0	0.0	1.0	0.06185
Na2	0.6143	0.0	0.25	0.01215	0.04571
Zr	0.0	0.0	0.14871	0.93548	0.03174
Ce	0.0	0.0	0.14871	0.01974	0.08746
P	0.2897	0.0	0.25	0.90784	0.07327
O1	0.1774	-0.02324	0.18624	1.01015	0.01871
O2	0.193	0.16051	0.08781	1.09178	0.09411
$NaZr_{1.9}Se_{0.1}P_3O_{12}$					
Na1	0.0	0.0	0.0	1.0	0.03185
Na2	0.6143	0.0	0.25	0.02774	0.05478
Zr	0.0	0.0	0.14871	0.80785	0.08865
Se	0.0	0.0	0.14871	0.02145	0.05489
P	0.2897	0.0	0.25	0.93784	0.06843
O1	0.1774	-0.02324	0.18624	1.07815	0.01491
O2	0.193	0.16051	0.08781	1.097	0.03925

Table 3. Inter-Atomic Distances ($Å$) for $NaZr_{1.9}Ce_{0.1}P_3O_{12}$ and $NaZr_{1.9}Se_{0.1}P_3O_{12}$ Polycrystalline Solid Solutions at Room Temperature

Bond lengths (Å)	$NaZr_{1.9}Ce_{0.1}P_3O_{12}$	$aZr_{1.9}Se_{0.1}P_3O_{12}$
Na1-O1	2.34728(7)*6	2.45001(5)*6
Na2-O2	2.32711(7)*2	2.32960(5)*2
Zr/Ce/Se-O1	2.026540(30)*3	2.07492(30)*3
Zr/Ce/Se O2	2.069750(30)*3	2.05177(30)*3
P-O1	1.517370(30)*2	1.51932(30)*2
P-O2	1.546730(30)*2	1.55423(30)*2

*Indicates multiplicity of the bonds. The values in parentheses denote (estimated standard deviation) ESD value.

Table 4. Inter-Atomic Bond Angles for $NaZr_{1.9}Ce_{0.1}P_3O_{12}$ and $NaZr_{1.9}Se_{0.1}P_3O_{12}$ Polycrystalline Solid Solutions at Room Temperature

O-M-O bond angles	$NaZr_{1.9}Ce_{0.1}P_3O_{12}$	$NaZr_{1.9}Se_{0.1}P_3O_{12}$
O1-Na1-O1	63.4294(10)*6	66.4321(10)*6
O2-Na1-O2	180.0*2,179.972	179.9802*3
O1-Na2-O1	113.5701(10)*5	114.5648(10)*5
O2-Na2-O2	115.5296(10)	114.5387(10)
O1-Zr-O1	89.9184(8)*3	90.5148(9)*3
O1-Zr-O2	91.1278(9)*3	92.4975(9)*3
O1-Zr-O2	173.9112(10)*3	175.8609(10)*3
O1-Zr-O2	90.7479(9)*3	91.7578(9)*3
O2-Zr-O2	83.2629(9)*3	85.8788(9)*3
O1-P-O1	108.8297(12)	106.5079(12)
O1-P-O2	107.70190(10)*2	106.69140(10)*2
O1-P-O2	113.1137(5)*2	112.0972(5)*2
O2-P-O2	107.8660	110.7178

The values in parentheses denote (estimated standard deviation) ESD value.

Modification in the bond distances and bond angles with substitution of Ce/Se can be clearly seen in the tables along with standard deviations. Bond distances are increased from 2.02 to 2.06 Å, during substitution of Zr by Ce. In contrast, bond distances are decreased from 2.07 to 2.05 Å with substitution of Zr by Se. The O-Zr-O angles vary between 83.262º and 175.911º. The angles implying the shortest bonds are superior to those involving the longest ones due to O-O repulsions which are stronger for O(1)-O(1) than that for O(1)-O(2). The P-O distances are close to those found in NASICON type phosphates. The O-P-O angles vary between 106.507º and 113.113º. The average bond distances of Na-O (2.43 Å) and P-O (2.05 Å) are greater than the previously published work (27). The oak ridge thermal ellipsoid plot program (ORTEP) view generated by the refined structural data shows two values of Zr-O distances namely Zr-O(1) and Zr-O(2) in multiple of 3 whereas P-O distances occur in two pairs (Fig. 4).

SEM and EDX Analyses

The microstructure of the title phase has been examined by SEM and EDAX analyses of the specimen. The morphology of SeNZP and CeNZP phase can be seen clearly in the electron micrographs of the ceramic sample (Fig. 5). Within the limits of experimental error, the EDAX analytical data on atomic and wt% of Na, Zr, P, Se and Ce are found agreeable with their corresponding expected molar ratios.

IR Analysis

The presence of orthophosphate anions in the crystal structure was confirmed by the infrared (IR) spectroscopy. The absorption bands in the region of 1280 cm^{-1} to 1020 cm^{-1} are assigned to the stretching asymmetric vibrations υ_3, and bands in the region of 980 cm^{-1} to 915 cm^{-1} correspond to the stretching symmetric vibrations υ_1 of the $(PO_4)^{3-}$ ions. Bands in the 670 cm^{-1}-400 cm^{-1} assigned to the bending vibrations υ_4 and υ_2. Similar data have been reported by Barj *et al*. [28]. Based on the analysis of the presented IR spectra, we assumed that phosphate of the $NaSe_{0.1}Zr_{1.9}P_3O_{12}$ and $NaCe_{0.1}Zr_{1.9}P_3O_{12}$ compositions to be characterized by the *R*-3*c* space group and the prepared samples can be

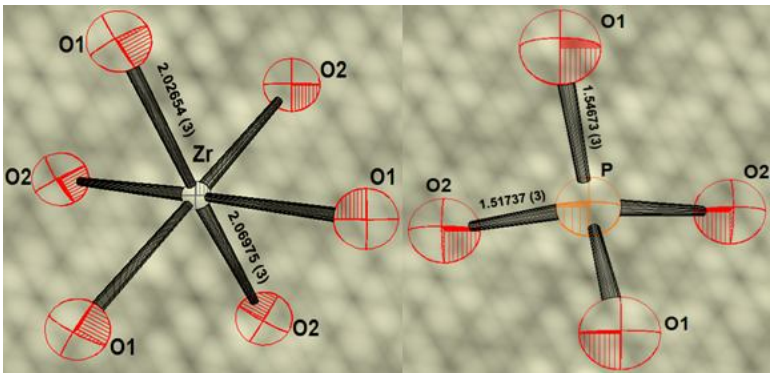

Fig. 4. ORTEP view of phosphorous and zirconium coordination in PO_4 tetrahedra and ZrO_6 octahedra in $NaCe_{0.1}Zr_{1.9}P_3O_{12}$.

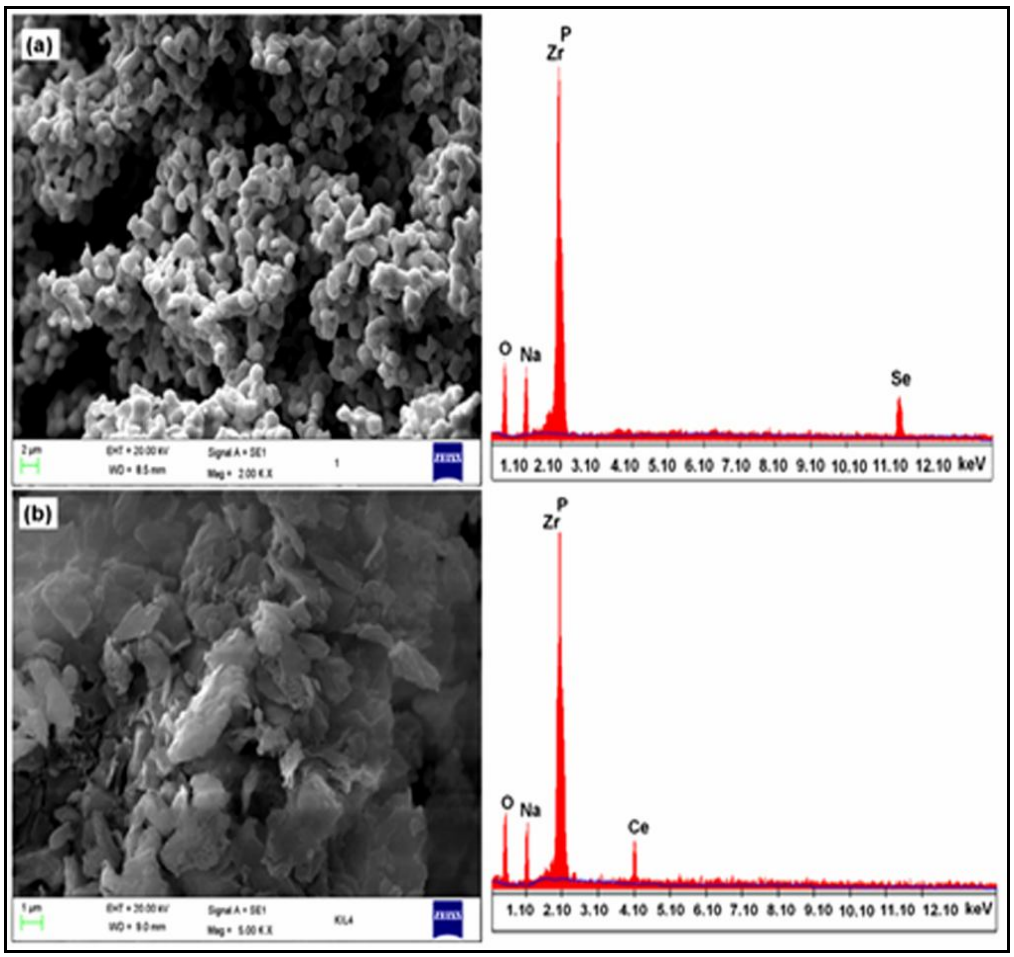

Fig. 5. (a) Scanning electron micrograph and EDAX spectrum of $NaSe_{0.1}Zr_{1.9}P_3O_{12}$ ceramic phases. (b) Scanning electron micrograph and EDAX spectrum of $NaCe_{0.1}Zr_{1.9}P_3O_{12}$ceramic phases.

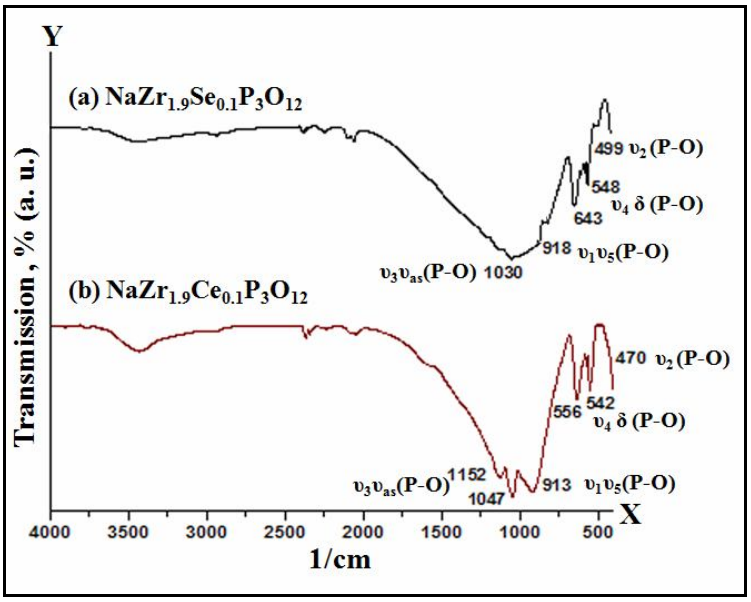

Fig. 6. Infrared spectra of $NaSe_{0.1}Zr_{1.9}P_3O_{12}$ and $NaCe_{0.1}Zr_{1.9}P_3O_{12}$ ceramic phases.

attributed to the orthophosphate class [28-34] (Fig. 6).

CONCLUSIONS

Refinement of powder X-ray diffraction data shows that the solid solutions of Se/Ce substituted sodium zirconium phosphate (NZP) prepared at 1250 °C crystallize in the rhombohedral (*R*-3c space group) structure and do not exhibit any phase transition. The conditions for the rhombohedral lattice were verified for all reflections. The structure refinement suggests that tetravalent Ce and Se are partially substitutes for zirconium *via* charge compensation being acquired by Na^+ in the structure. Crystal data and structural parameters of the material have been refined to a satisfactory convergence with reasonable values of Rietveld parameters (Rp & Rwp). The calculated values of P-O, Zr-O bond lengths and O-M-O bond angles are in good agreement with the expected values. NZP has been identified as a potential material for immobilization and solidification of cerium and selenium from intermediate level waste from LWR fuel reprocessing. The structure model also calculated the atomic distances of this cost effective immobilization matrix for intermediate level nuclear waste of the fuel reprocessing plants.

REFERENCES

[1] G. Roth, S. Weisenburger, Nucl. Eng. Des. 202 (2000) 197.
[2] C. Rodney, Ewing; Ceram. Int. 17 (1991) 287.
[3] H.T. Hawkins, B.E. Scheetz (Eds.), in: Proceedings of the Material Research Society, Fall Meeting, Boston, MA, 1996.
[4] I.W. Donald, B.L. Metcalfe, R.N.J. Taylor, J. Mater. Sci. 32 (1997) 5851.
[5] S. Pratheep Kumar, G. Buvaneswari, R. Madhavan, G.K.V. Kutty, Radiochemistry 53 (2011) 421.
[6] R. Chourasia, O.P. Shrivastava, R.D. Ambashta, P.K. Wattal, Ann. Nucl. Energy 37 (2010) 103.
[7] A.E. Ringwood, S.E. Kesson, N.G. Ware, W. Hibberson, A. Majar, Nature 278 (1979) 219.
[8] B.C. Sales, L.A. Boatner, Mater. Lett. 2 (1984) 301.
[9] M.L. Carter, H. Li, Y. Zhang, E.R. Vance, D.R.G. Mitchell, J. Nucl. Mater. 384 (2009) 322.
[10] B.E. Scheetz, D.K. Agrawal, E. Breval, R. Roy, Waste Manage. 14 (1994) 489.
[11] A.I. Orlova, V.A. Orlova, M.P. Orlova, Radiochemistry 48 (2006) 330.
[12] G. Buvaneswari, K.V. Govindan Kutty, U.V.

Varada-Raju, Mater. Res. Bull. 39 (2004) 475.
[13] E. Breval, H.A. McKinstry, D.K. Agrawal, J. Mat. Sci. 35 (2000) 3359.
[14] J. Alamo, R. Roy, J. Mater. Sci. 21 (1986) 444.
[15] V.I. Petkov, E.A. Asabina, Glass Ceram 61 (2004) 233.
[16] M.V. Sukhanova, V.I. Pet'kov, D.V. Firsov, Russ. J. Inorg. Chem. 56 (2011) 1351.
[17] R. Rustam, E.R. Vance, Alamo J. Mater. Res. Bull 17 (1982) 585.
[18] JCPDS Powder Diffraction Data File no. 71-0959 Compiled by International Center for Diffraction Data, USA, 2000.
[19] A.C. Larson, R.B. Von Dreele, LANSCE, MS-H805, Los Almos National Laboratory LAUR (2000) 86.
[20] B.H. Toby, J. Appl. Crystallog. 34 (2001) 210.
[21] H.M. Rietveld, J. Appl. Cryst. 2 (1969) 65.
[22] H. Kojitani, M. Kido, M. Akaogi, Phys. Chem. Miner. 32 (2005) 290.
[23] C. Verissimo, F.M.S. Garrido, O.L. Alves, P. Calle, A.M. Juarez, J.E. Iglesias, J.M. Rojo, Solid State Ionics 100 (1997) 127.
[24] G.E. Lenain, H.A. McKinstry, J. Alamo, D.K. Agrawal, J. Mat. Sci. 22 (1987) 17.
[25] L. Hagman, P. Kierkegaard, Acta Chem. Stand. 22 (1968) 1822.
[26] R.D. Shannon, Acta Crystallogr. A-32 (1976) 751.
[27] J.P. Boilot, G. Collin, P. Colomban, J. Solid State Chem. 73 (1988) 160.
[28] M. Barj, Perthuis, P. Colomban, Solid State Ionics 9 & 10 (1983) 845.
[29] O.P. Shrivastava, R. Chourasia, N. Kumar, Ann. Nucl. Energy 35-36 (2008) 1147.
[30] V.I. Pet'kov, E.A. Asabina, A.V. Markin, N.N. Smirnova, J. Therm. Anal. Calorim. 91 (2008) 155.
[31] E.Y. Borovikova, V.S. Kurazhkovskaya, D.M. Bykov, A.I. Orlova, J. Struct. Chem. 51 (2010) 40.
[32] G. Buvaneswari, U.V. Varadaraju, J. Solid State Chem. 145 (1999) 227.
[33] M. Barj, H. Perthuis, P. Colomban, Solid State Ionics 11 (1983) 157.
[34] A. Mbandza, E. Bordes, P. Courtine, Mater. Res. Bull. 20 (1985) 251.